RSC Advances

PAPER

View Article Online
View Journal | View Issue

Published on 12 December 2014. Downloaded by Michigan State University on 21/01/2016 06:19:26.

Cite this: *RSC Adv.*, 2015, **5**, 5988

Preparation of multi-shell structured fluorescent composite nanoparticles for ultrasensitive human procalcitonin detection†

Yue Zhao,[a] Changhua Zhou,*[ac] Ruili Wu,[ac] Lin Li,[b] Huaibin Shen[ac] and Lin Song Li*[ac]

Received 29th October 2014
Accepted 12th December 2014

DOI: 10.1039/c4ra13362e

www.rsc.org/advances

In this paper, we reported the preparation of carboxyl functionalized quantum dots (QDs)-embedded silica nanoparticles by combining layer-by-layer (LbL) self-assembly technique and a multi-layer protection method. Preformed SiO_2 nanoparticles synthesized *via* the Stöber method were first alternately deposited with positively charged polyelectrolyte (poly(diallyl dimethylammonium chloride), PDDA) and negatively charged CdSe/ZnS QDs by LBL method and further coated by a silica shell. Then, the functionalization of SiO_2@PDDA@QDs@SiO_2 nanoparticles with hydrophobic hydrocarbons and biocompatible oligomers impart optical imaging properties and good colloidal stability in aqueous solutions at a wide range of pH, PBS buffer, and under thermal treatment. In addition, these newly developed multi-shell structured nanoparticles coupled with specific antibodies were successfully applied in detecting procalcitonin (PCT) antigens using fluorescent lateral flow immunoassay (LFIA). The naked-eye detection limit of fluorescence nanoparticles could achieve 0.1 ng mL^{-1} of PCT antigens, which was about two hundred times higher than that of colloidal gold-based method.

1. Introduction

Multiplex and high-throughput assays are becoming an essential platform for biomedical imaging, diagnostics, therapy and so on.[1–4] In all these areas, considerable attention has focused on the development of fluorescence-encoded multiplex technology as fluorescent labels.[5] So far, both organic and inorganic quantum dots (QDs) were widely used as fluorescent labels. Compared to organic fluorophores, QDs have their outstanding photophysical properties such as narrow and size-tunable emission spectra, a robust signal intensity, a broad excitation band, and high photochemical stability.[6–9] Especially, with respect to bioapplications, they provide unrivalled cellular imaging and therapeutic detection capabilities.[10] However, in practical applications, separation and stability of QDs is difficult to control and deal with, remaining an issue to be solved in the field of biotechnological applications. A promising way to solve these problems is the incorporation of QDs into substrates.[6–14] Recently, QDs could be incorporated into microbeads during synthesis, entrapped by solvent swelling or deposited by a layer-by-layer (LbL) adsorption technique.[15–18] Compared with the above two methods, polyelectrolyte multilayer microspheres prepared by the LbL technique have advantages of its simplicity, well-controlled size and shape, finely tunable multilayer thickness, variable compositions and functions.[19] The LbL-assembled films of negatively charged colloidal SiO_2 nanoparticles and a suitable polycation was first reported in detail by Cebeci *et al.*[20] Gao and co-workers successfully obtained multiplexed optical encoding microbeads by incorporating water-soluble CdTe QDs into polystyrene microspheres. Wang, Gao, and colleagues used LbL technique to incorporate QDs into poly(*N*-isopropylacrylamide) (PNIPAM) hydrogel spheres.[21,22] Among of these supports, silica is one of the most used materials in nanotechnology, which provides a stable and accessible surface for immobilizing a variety of functional molecules and small particles.[23,24] Besides optical coding methods, surface functional groups and stability are also vital to the applications of QD-encoded beads. Therefore, exploring an efficient route for building up functional nanoprobes with both stable fluorescence and a modifiable surface is still in urgent demand for biological applications.

Herein, we reported the preparation of carboxyl functionalized QD-embedded silica nanoparticles by combining layer-by-layer (LbL) self-assembly technique and a multi-layer protection method. First, the obtained negatively charged silica spheres were ready as templates for the subsequent preparation.[25] The positively charged polyelectrolyte (poly(diallyldimethylammonium chloride), PDDA) and polymaleic acid *n*-hexadecanol ester (PMAH) functionalized CdSe/ZnS QDs (QDs–PMAH) were alternately adsorbed onto the silica spheres.

[a]*Key Laboratory for Special Functional Materials of the Ministry of Education, Henan University, Kaifeng, 475004, P. R. China. E-mail: changhua@henu.edu.cn; lsli@henu.edu.cn; Fax: +86-371-23881358; Tel: +86-371-23881358*

[b]*Autobio Diagnostics Co., Ltd, Zhengzhou, 450016, P. R. China*

[c]*Collaborative Innovation Center of Nano Functional Materials and Applications, Henan Province, P. R. China*

† Electronic supplementary information (ESI) available. See DOI: 10.1039/c4ra13362e

This journal is © The Royal Society of Chemistry 2015

Published on 12 December 2014. Downloaded by Michigan State University on 21/01/2016 06:19:26.

Finally, multi-layer protection from silica shell and amphiphilic polymer layers was introduced on SiO_2@PDDA@QDs nanoparticles.[26] The resulting SiO_2@PDDA@QDs@SiO_2@OTMS@PMAH nanoparticles showed excellent stability (pH, PBS buffer, and under thermal treatment) in aqueous solution. In addition, we attempted to use the obtained multi-shell structured fluorescent nanoparticles to detect procalcitonin (PCT) antigen based on a lateral flow immunoassay (LFIA) biosensor system.

2. Experimental

2.1 Materials

All reagents were used as received without further experimental purification. Cadmium oxide (CdO, 99.99%), sulfur (S, 99.98%), 1-octadecene (ODE, 90%), oleic acid (OA, 90%), selenium (Se, 99.99%), zinc oxide (ZnO, 99.99%), trimethoxy(octadecyl)silane (OTMS), and poly(diallyl dimethylammonium chloride) (PDDA, 20%) were purchased from Aldrich. *N*-Hexane (95%), *n*-butanone (99.5%), methanol (99.5%), ethanol (analytical grade), maleic anhydride (MA, 99.5%), acetone (99.5%), benzoyl peroxide (BPO, 98.0%), methylbenzene (99.5%) were obtained from Kermel. Sodium chloride (NaCl), hydrochloric acid (HCl), and sodium hydroxide (NaOH) were all of analytical grade and obtained from Sagon Biotech Co., Ltd. Acetic acid, tetraethyl orthosilicate (TEOS), and ammonia (28%) were obtained from Beijing Chemical Reagent Ltd., China. Deionized water was used for all experiments.

2.2 Apparatus

The size and morphology of the nanoparticles were investigated using a JEM 100CX-II transmission electron microscope (TEM) at 100 kV. Room-temperature photoluminescence (PL) spectra were measured with an Ocean Optics spectrophotometer (mode PC2000-ISA) with wavelength ranging from 300 to 800 nm. PL spectrum was taken using an excitation wavelength of 365 nm. The hydrodynamic sizes and zeta potential of PL nanoparticles were obtained from a dynamic light scattering (DLS, Malvern Instruments Corporation, Nano ZS) at 25 °C. X-ray diffraction (XRD) studies of nanoparticles were carried out with a Philips X'Pert Pro X-ray diffractometer using Cu Ka radiation.

2.3 Synthesis of sandwich-like structured SiO_2@PDDA@QDs@SiO_2@OTMS@PMAH nanoparticles

2.3.1. Preparation of water-soluble CdSe/ZnS QDs. High quality red-emitting hydrophobic CdSe/ZnS QDs (PL 610 nm) could be prepared in organic solution *via* previously reported procedures (details in ESI†).[27,28] The obtained QDs were purified by precipitation in acetone and then methanol, and redispersed in $CHCl_3$. The absorption and PL spectra of the hydrophobic CdSe/ZnS QDs were shown in ESI (Fig. S1†). The procedure for the preparation of aqueous CdSe/ZnS QDs was as follows:[29] firstly, 0.02 mmol of QDs dispersed in 1 mL of $CHCl_3$ were added to a solution containing 0.16 mmol of PMAH dispersed in 10 mL of $CHCl_3$, and the resulting dispersion was stirred for 24 h in a closed container. Then, $CHCl_3$ solvent was removed under vacuum, and the remaining QDs film was dispersed in ammonia water (pH = 9) with sonication to obtain a QDs solution. To remove possible larger contaminants, the solution was passed through a 0.22 μm nylon syringe filter. Excess PMAH oligomer was removed through centrifugation (30 000 rpm for 30 min). The negatively charged (carboxyl groups modified) QDs could be further operated by LbL self-assembly technique.

2.3.2. Synthesis of mono-dispersed silica as spherical supports. Uniformly sized silica spheres[30] were prepared as follows: 4.5 mL of ammonia solution (28%), 8.2 mL of acetone solution and 14 mL of deionized water was added to a flask under vigorous stirring to form solutions A. Solutions B was obtained by mixing 4.5 mL of TEOS and 22.4 mL of acetone solution under sonication for 10 min. Afterward, solution B was added into solution A in the flask under rapid stirring at room temperature and reacted for 2 h. The excess unreacted reagents were removed by centrifugation (7000 rpm, 5 min) and washed in sequence with acetone and deionized water. The resultant silica spheres were dispersed in 20 mL of deionized water.

2.3.3. Preparation of SiO_2@PDDA@QDs. SiO_2@PDDA@QDs nanoparticles were prepared by linking the negatively charged QDs and silica spheres with a positive polyelectrolyte through electrostatic interaction. When the optimum pH value was about 5, 0.2 mL of SiO_2 solution (0.12 g mL^{-1}) and 8 mL of cationic PDDA solution (2.0 M, 0.5 M NaCl) were mixed under sonication for 30 min. In order to remove non-adsorbed polyelectrolytes, this mixture was centrifuged twice at 7000 rpm for 5 min in deionised water. Polyelectrolyte adsorption time of 30 min was sufficient for adsorption saturation. Longer adsorption time had no effect on the zeta potential values.[31] Afterward, the positively charged silica spheres were dispersed into a PMAH-coated QDs solution (0.005 g), and sonicated for another 30 min. Then, the solution was centrifuged for 5 min at 7000 rpm to remove excess QDs solution. SiO_2@PDDA nanoparticles coated with one layer of QDs were obtained by three centrifugation/washing cycles.

2.3.4. Synthesis of SiO_2@PDDA@QDs@SiO_2. The obtained SiO_2@PDDA@QDs nanoparticles were incorporated into silica shell by a conventional Stöber method.[32] In a typical procedure, 2.0 mL of SiO_2@PDDA@QDs solution was added to 20 mL of anhydrous ethanol, followed by the addition of 15 μL TEOS and 200 μL ammonia solution (28%). The mixture was stirred at 25 °C for 8 h. The SiO_2@PDDA@QDs@SiO_2 nanoparticles were then purified by performing three cycles of centrifuging, discarding the supernatant, and redispersing the microspheres in ethanol.

2.3.5. Hydrophobic modification of SiO_2@PDDA@QDs@SiO_2 nanoparticles. The obtained silica-coated luminescent nanoparticles were further modified by adding trimethoxy(octadecyl)silane (OTMS) in ethanol/chloroform mixture. In detail, 200 μL of ammonia solution (28%) was added into the SiO_2@PDDA@QDs@SiO_2 solution (20 mL, dispersed in anhydrous ethanol). 2.5 mL of OTMS solution (10%, dispersed in $CHCl_3$) was then dropwisely added into the SiO_2@PDDA@QDs@SiO_2 suspension under vigorous stirring. This reaction was lasted for 24 h at 25 °C. At the end of the reaction, the preformed nanoparticles were washed with ethanol to eliminate excess reactants by centrifugation and dispersed in 1 mL of $CHCl_3$.

Published on 12 December 2014. Downloaded by Michigan State University on 21/01/2016 06:19:26.

2.3.6. Synthesis of carboxylic-functionalized SiO_2@PDDA@QDs@SiO_2@OTMS@PMAH nanoparticles. The surface of SiO_2@PDDA@QDs@SiO_2@OTMS nanoparticles were functionalized with carboxylic groups by treating with PMAH.[25] 0.1 g PMAH was dissolved in 5 mL $CHCl_3$, followed by the addition of QDs–PMAH–SiO_2–OTMS nanoparticles into the system and stirred for 24 h in a closed container. Afterwards, $CHCl_3$ was then slowly evaporated under vacuum, and the reaction product was dispersed in 2.0 mL ammonia water (pH = 9) with sonication. The solution was centrifuged for 10 min at 1200 rpm to remove excess PMAH. The resulting SiO_2@PDDA@QDs@SiO_2@OTMS@PMAH nanoparticles were readily redispersed into water.

2.3.7. Conjugation of antibodies onto water-soluble nanoparticles. The carboxylic-functionalized SiO_2@PDDA@QDs@SiO_2@OTMS@PMAH nanoparticles were readily reacted with the amino groups of the protein by using *N*-(3-dimethylaminopropyl)-*N*-ethylcarbodiimde hydrochloride (EDC) and *N*-hydroxysuccinimide (NHS) as zero-length cross-linkers. The as-prepared water-soluble nanoparticles were regulated to pH 5.0 with MES buffered saline, then 50 μL EDC (20 mg mL^{-1}) and 50 μL sulfo-NHS (60 mg mL^{-1}) were added and blended by vortex. The mixed solution was then incubated at 25 °C for 15 min to fully activate the multi-shell structured nanoparticles. The nanoparticles were then centrifuged at 5000 rpm for 10 min, the supernatant was discarded. After washing with 50 mM MES buffer (pH = 5.5) and the process repeated twice in order to remove the possible unreacted reagents. 400 μL PCT antibody solution (1 mg mL^{-1}) was dispersed to activated water-soluble nanoparticles for reaction for 2 h at 37 °C to result in stable amide bonds between the antibodies and the water-soluble nanoparticles. Blocking with 40 μL 10% BSA solution in 0.05 M MES buffer (pH = 5.5) at room temperature for another 1 h, the conjugates solution was further centrifuged (5000 rpm, 10 min) and diluted by 1 mL 1% BSA in PBS buffer for two times to completely remove the impurities. The precipitates were dissolved by PBS containing 1% BSA and 1% sucrose and then stored at 4 °C for use.

2.3.8. Preparation of lateral flow test strips. PCT antibody in 30 mM PBS (pH = 7.4) was dispensed onto the test line of the nitrocellulose membrane with the XYZ dispenser at concentration of 1 mg mL^{-1}. Goat-anti-mouse antibody was dispensed on the top of the membrane as control line. After drying for 30 min, the nitrocellulose membrane was blocked with PBS containing 0.2% TWEEN-20 (w/v). The composite-antibody was printed on conjugate pad and dried at room temperature. All of the parts were assembled on a plastic adhesive backing card in order with proper overlapping distance. Then the whole card was cut into final test strips of 4 mm in width with guillotine cutter and assembled into a strip cassette for the following assay.

2.3.9. Detection of PCT antigen by nanoparticles-LFIA strips. The composite nanoparticles-based lateral flow immunoassay was developed as a rapid visual quantitative test which rather than just gave a simple yes/no response to the levels of the target analytes. Therefore, to perform the PCT antigen detection, 80 μL of the PCT antigen solution was added to the end of sample pad, the fluorescence signal of composite nanoparticles on the test line was observed by the spectrofluorometer after excitation. The nanoparticles-LFIA assays were performed at various concentrations of PCT antigen: 0, 0.1, 0.25, 0.5, 3.5, 6, 8, and 10 ng mL^{-1}, respectively.

3. Results and discussion

3.1. Synthesis of SiO_2@PDDA@QDs@SiO_2@OTMS@PMAH nanoparticles

The fabrication flow of the proposed, highly bright QDs-embedded silica nanoparticles with uniform size and composition by the LbL self-assembly technique and a multi-layers protection method is illustrated in Scheme 1. Silica spheres could be created through the classical Stöber method, which usually relies on sol–gel chemistry involving the hydrolysis of TEOS in an alcohol/water solution using ammonia as the catalyst.[33] The LbL assembly approach require water-soluble QDs, the as-prepared hydrophobic CdSe/ZnS QDs could be water solubilized by using a PMAH-mediated encapsulation method as reported previously. In addition, the pH value of solution is also highlighted as an important factor to achieve sufficient QD surface coverage. We optimized the process of synthesis at the correct pH conditions, resulting in a higher QD coverage after three wash cycles. First, negatively charged SiO_2 particles were reversed the surface charge by adsorbing positively charged PDDA at pH 5.0. Then, SiO_2@PDDA@QDs particles were prepared by linking the positive charged SiO_2@PDDA and negatively charged QDs at pH value of 9.0 through electrostatic interaction. Afterwards, another silica protecting layer was coated on the SiO_2@PDDA@QDs to prevent the QD_S from off the SiO_2@PDDA nanoparticles and improve the stability in harsh environments. To satisfy the requirement of biocompatibility, the surfaces of the SiO_2@PDDA@QDs@SiO_2 nanoparticles were further passivated using OTMS, which changed the SiO_2@PDDA@QDs@SiO_2 from hydrophilic to hydrophobic and provided an additional protection. Afterwards, the hydrophobic SiO_2@PDDA@QDs@SiO_2@OTMS nanoparticles were converted back to water-soluble again by grafting the hydrophobic surface with PMAH. The obtained carboxylic-functionalized nanoparticles could enable further conjugation of targeting biomolecules.

The morphology and size of CdSe/ZnS QDs before (a) and after (b) phase transfer were characterized by TEM and shown in Fig. 1. The hydrophobic QDs were nearly monodisperse with an average diameter of 9.8 nm in $CHCl_3$. After phase transfer, the hydrophilic QDs in water still remained monodisperse in size and no obvious shape change and aggregation were observed. Fig. 1(c) showed the TEM image of silica nanoparticles with an average diameter of about 220 nm. A closer TEM image of a single nanoparticle was demonstrated in Fig. 1(d), which clearly indicated silica nanoparticle surfaces were smooth. The morphology and size of SiO_2@PDDA@QDs were characterized by TEM in Fig. 1(e). It is clearly showed that their surfaces were evenly covered by QDs, and the QD-doped silica nanoparticle surfaces were comparatively rough. A closer image of a single particle was demonstrated in Fig. 1(f), which indicated the

 This journal is © The Royal Society of Chemistry 2015

Published on 12 December 2014. Downloaded by Michigan State University on 21/01/2016 06:19:26.

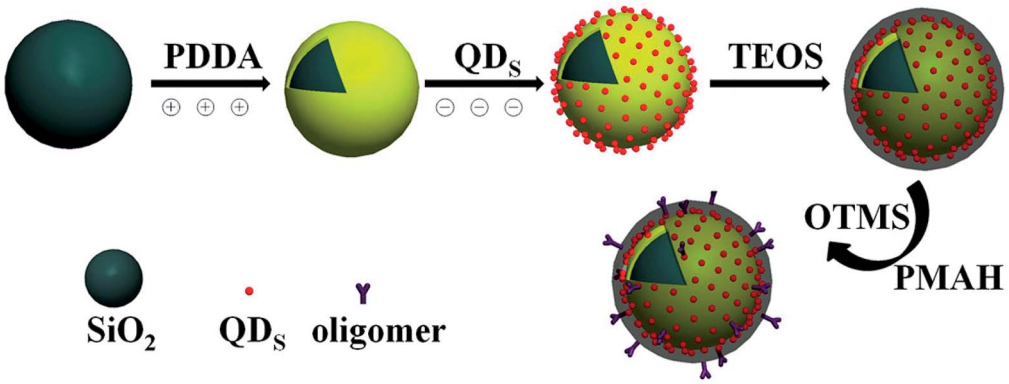

Scheme 1 Schematic illustration of a multi-shell protecting procedure for the synthesis of SiO_2@PDDA@QDs@SiO_2@OTMS@PMAH nanoparticles.

number of QDs on the SiO_2@PDDA was estimated to be ≈400–900 per single PDDA-coated SiO_2 nanoparticle. TEM image (Fig. 1(g)) exhibited the efficacy of the Stöber method in encapsulating the SiO_2@PDDA@QDs nanoparticles within silica. All the samples of silica-coated SiO_2@PDDA@QDs nanoparticles appeared to be uniform in size and well dispersed. From the zoomed image of Fig. 1(h), a single SiO_2@PDDA@QDs nanoparticle with a 15 nm thick silica layer could be clearly seen. By controlling the concentration of SiO_2@PDDA@QDs nanoparticles and the hydrolysis of TEOS, the SiO_2@PDDA@QDs nanoparticles with tunable silica shells could be prepared.[34] In our study, the silica shell thickness could be tuned in the range of 15–30 nm (Fig. S2†). After further surface modification with OTMS and PMAH, these layers are not visible under TEM because the organic molecules are not electron-dense materials. Apparently, the multistep modification processes did not cause the aggregation of nanoparticles, which was also confirmed by dynamic light scattering (DLS) measurement in an aqueous environment.

The hydrodynamic size distribution changes in the preparation of SiO_2@PDDA@QDs@SiO_2@OTMS@PMAH nanoparticles could be monitored in real time by dynamic light scattering (DLS). Beyond a dimensional change, the dispersion of the nanospheres was observed in solution.[35] As shown in Fig. 2(a) of the information, the hydrodynamic diameters (HD) of SiO_2, SiO_2@PDDA, SiO_2@PDDA@QDs and SiO_2@PDDA@QDs@SiO_2 were 245.9, 316.4, 305.1 and 272.3 nm, respectively, which were larger than the measured diameters from the TEM images. The DLS result showed a HD of 396.1 nm for SiO_2@PDDA@QDs@SiO_2@OTMS@PMAH nanoparticles, which was much larger than the nanoparticles produced in the process of the former. This is because PMAH provided plentiful carboxylic acid groups on nanoparticles surface in order to carry with the high negative charges in water. This negative surface

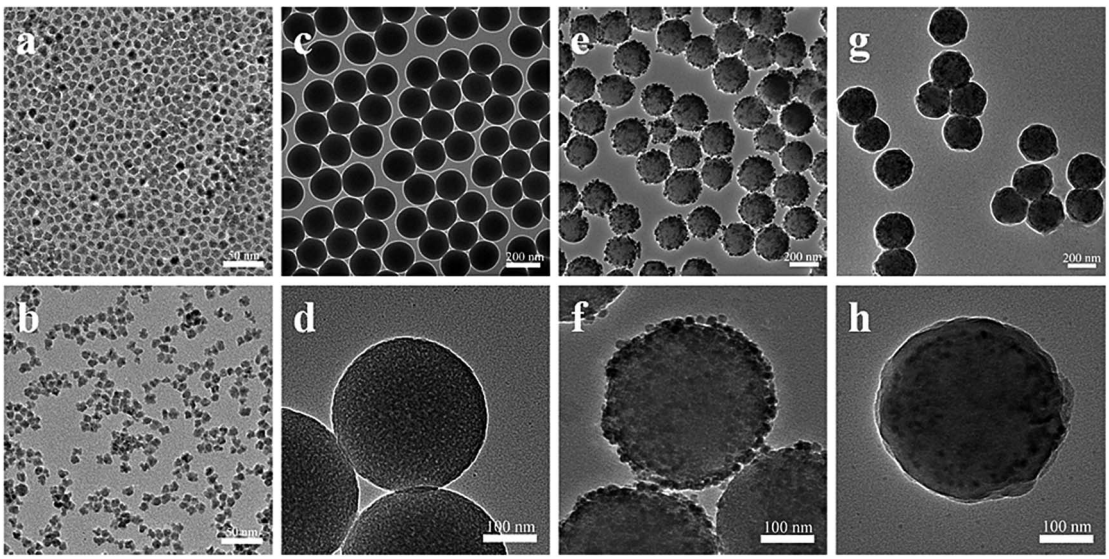

Fig. 1 TEM images of CdSe/ZnS quantum dots before (a) and after (b) phase transfer; (c) TEM image of SiO_2 nanoparticles; (d) TEM image of a single SiO_2 nanoparticle; (e) TEM image of SiO_2@PDDA@QDs nanoparticles; (f) TEM image of a single SiO_2@PDDA@QDs nanoparticle; (g) TEM image of SiO_2@PDDA@QDs@SiO_2 nanoparticles; (h) TEM image of a single SiO_2@PDDA@QDs@SiO_2 nanoparticle.

Published on 12 December 2014. Downloaded by Michigan State University on 21/01/2016 06:19:26.

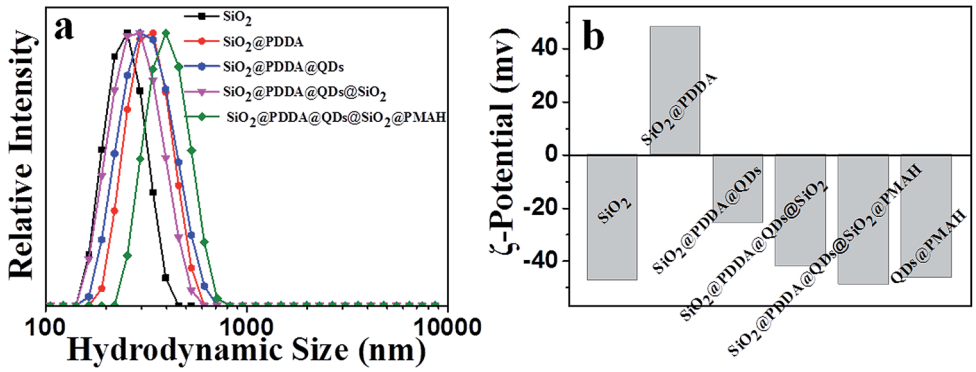

Fig. 2 (a) Comparing the DLS data of nanoparticles at different stages; (b) zeta potential changes in the preparation of SiO_2@PDDA@QDs@SiO_2@OTMS@PMAH nanoparticles.

charge not only increased the colloidal HD compared to the natural size, but also created an electrical double layer in aqueous solution to prevent QDs from aggregation.

Furthermore, zeta-potential measurements were used as a second independent method to confirm multilayer formation (Fig. 2(b)). The zeta potential of silica nanoparticles showed a negatively surface charge of −47.4 mV. The presence of PDDA, which is cationic, caused a reversal in zeta potential to 48.2 mV. Subsequent deposition of PMAH coated QDs onto the SiO_2@PDDA nanoparticles made surface charge neutralization to a value of −25.6 mV. SiO_2@PDDA@QDs particles were encapsulated by SiO_2 shell, and zeta potential measured in water is −42.0 mV. The carboxylic functionalized SiO_2@PDDA@QDs@SiO_2@OTMS@PMAH nanoparticles added up to −49.0 mV. Multilayer coated silica particles were demonstrated by the alternating sign of the surface electric potential.

To further prove the growth of CdSe/ZnS QDs shell, the X-ray diffraction (XRD) pattern was used to indicate the existence of QDs in SiO_2@PDDA@QDs composites. Fig. 3 displayed the XRD pattern of SiO_2 and corresponding SiO_2@PDDA@QDs nanoparticles. At 2θ values of 22.45°, there appeared a wide peak in SiO_2 and SiO_2@PDDA@QDs particles respectively, which can be indexed to SiO_2 spheres. In the case of SiO_2@PDDA@QDs, three obvious XRD diffraction peaks are located at 26.45°, 43.83°, and 52.50° corresponding to (111), (220), and (311) planes of the CdSe/ZnS QDs. So CdSe/ZnS QDs were coated successfully on the surface of SiO_2@PDDA@QDs nanoparticles.

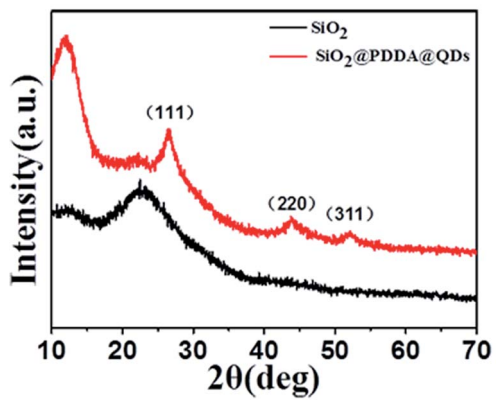

Fig. 3 XRD patterns of SiO_2 and SiO_2@PDDA@QDs.

PL study is a powerful tool to investigate the optical properties of these novel fluorescent nanoparticles. During different preparation stages, the changes of emission peak and intensity were shown in Fig. 4. The PL spectrum of the hydrophobic CdSe/ZnS QDs in $CHCl_3$ has a maximum peak at 610 nm and narrow FWHM with 34 nm. CdSe/ZnS QDs in different preparation stages exhibited a slightly red-shifted (<2 nm) emission peak from that of the original hydrophobic QDs (Fig. 4(a)). And the peak width of CdSe/ZnS QDs were the same as before encapsulation. At the meantime, PL intensity of original CdSe/ZnS QDs was slightly reduced (about 14%) after the transfer, adsorption, and coating process (Fig. 4(b)). These results indicated that CdSe/ZnS QDs were assembled on SiO_2 particle surface without PL changes associated with agglomeration, ripening, or changes in refractive index at the QD surface.

3.2. Stability tests of aqueous SiO_2@PDDA@QDs@SiO_2@OTMS@PMAH nanoparticles in physiological conditions

The stability and optical properties of SiO_2@PDDA@QDs@SiO_2@OTMS@PMAH under various biologically relevant conditions of pH, temperature, and PBS buffer were further examined (Fig. 5). Previously a number of groups have built QD-based pH sensors because QDs are sensitive to chemicals in the surrounding environment such as acids, bases, ions, and proteins. For example, pH values can be directly correlated with QD PL intensity because QD fluorescence, in general, is quenched in acids and is enhanced in bases. Next, we systematically studied the influence of pH values on stability of SiO_2@PDDA@QDs@SiO_2@OTMS@PMAH nanoparticles. The pH value of the SiO_2@PDDA@QDs@SiO_2@OTMS@PMAH solution was varied by dropwise addition of HCl or NaOH. Remarkably, the nanoparticles preserved high photostability and strong PL in the wide pH range 6–12. Such great improvement of pH stability was attributable to the distinctive surface properties of the silica and amphiphilic polymer multilayer shell. In addition, the PL intensity of our

 This journal is © The Royal Society of Chemistry 2015

Published on 12 December 2014. Downloaded by Michigan State University on 21/01/2016 06:19:26.

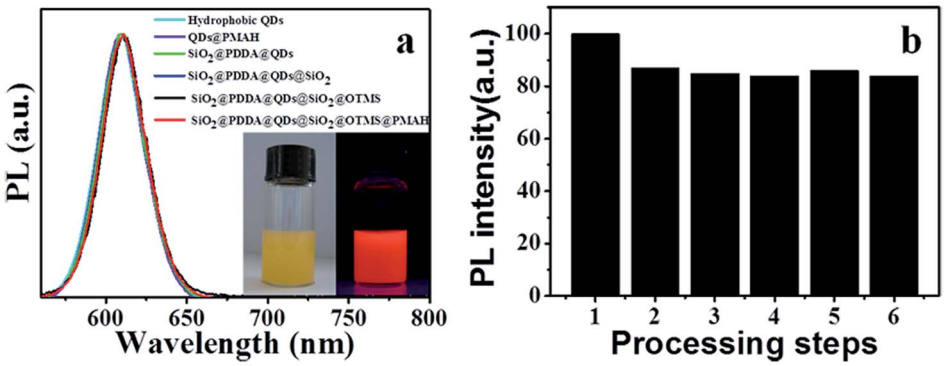

Fig. 4 Comparison of PL emission peak (a) and intensity (b) of SiO_2@PDDA@QDs@SiO_2@OTMS@PMAH nanoparticles at different stages. The inset of (a) is the photographs of the SiO_2@PDDA@QDs@SiO_2@OTMS@PMAH suspension under room light and UV light of 365 nm.

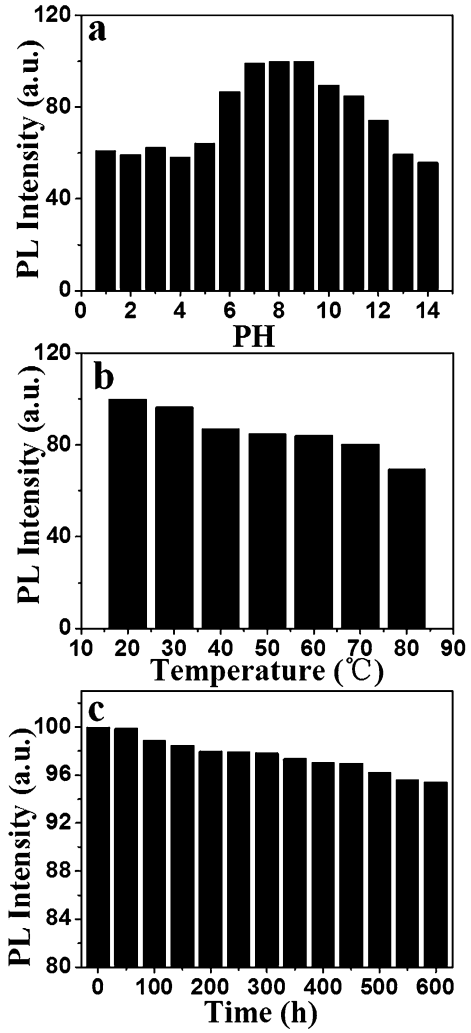

Fig. 5 pH (a), temperature (b) and PBS buffer (c) stability comparison of SiO_2@PDDA@QDs@SiO_2@OTMS@PMAH nanoparticles. The solution was incubated for 1 h before the pH and temperature stability test.

SiO_2@PDDA@QDs@SiO_2@OTMS@PMAH nanoparticles changed by less than 55% at pH 1 and 14 after 1 h incubation.

Temperature is another important parameter for biological experiments. Fig. 5(b) showed the variation of PL intensity of SiO_2@PDDA@QDs@SiO_2@OTMS@PMAH nanoparticles after heating. Although there was clear temperature dependence, the nanoparticles retained about 70% of their initial PL intensity even after being heated to 80 °C. Over the temperature range of most relevance to biological experiments (20 °C to 40 °C), the PL intensity varied by less than 15%.

These nanoparticles also exhibited stable PL when dispersed in common buffers like PBS buffer (pH = 7.2). As shown in Fig. 5(c), the PL intensity of SiO_2@PDDA@QDs@SiO_2@OTMS@PMAH nanoparticles only decreased slightly (<5%) and became constant after 600 h. These data suggest the potential of these nanoparticles as robust biomarkers due to their stronger fluorescence and better stability.

3.3. Demonstration of the SiO_2@PDDA@QDs@SiO_2@OTMS@PMAH nanoparticles as fluorescence labels for detecting PCT antigen

Human procalcitonin (PCT) is a biomarker that reacts with high sensitivity and specificity to generalized infection and sepsis.[36,37] It correlates better than all other existing parameters to the inflammatory activity of the immune system and can be used to diagnose and to monitor severe bacterial infections and sepsis. PCT supports early diagnosis and clinical decision making which could direct an effective therapy at the right time and avoid unnecessary spending for critically ill patients. Therefore, it is necessary to develop new high sensitivity detection method to detect PCT.

To explore the feasibility of composite nanoparticles in PCT antigen detection, we conjugated the obtained high fluorescent nanoparticles with PCT antibody using standard carbodiimide cross-linking reaction and designed an immuno-sandwich assay for PCT antigen detection. During the assay (as shown in Scheme 2),[38] aqueous sample was applied to the sample pad and transported to the conjugation zone, where the pre-absorbed and dried composite-antibodies were rehydrated and washed off and composite-antibody were formed. The sample

Published on 12 December 2014. Downloaded by Michigan State University on 21/01/2016 06:19:26.

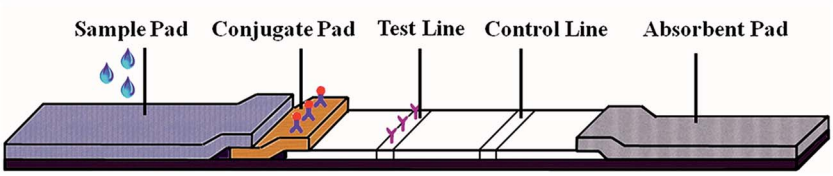

Scheme 2 Schematic representation for the LFIA system.

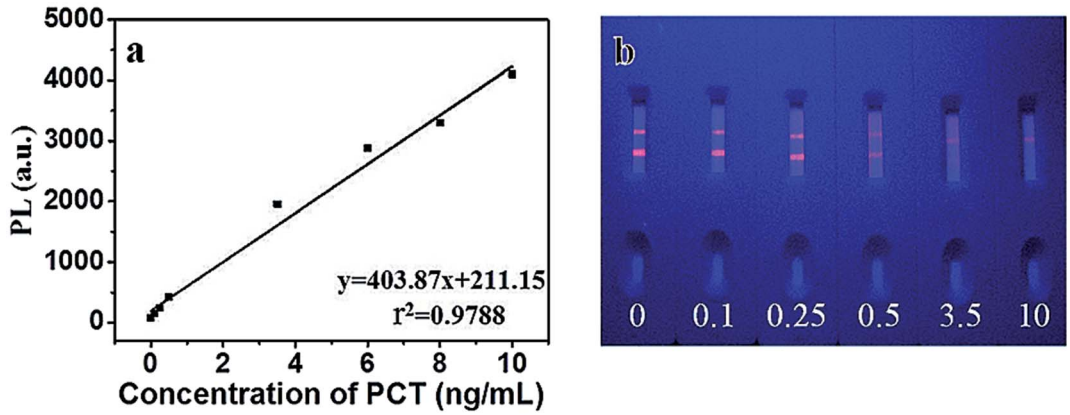

Fig. 6 QDs-based LFIA linear response (a) and typical photo image of detection results by the fluorescent strip under the ultraviolet irradiation (b).

further migrated to the test line where the second antibodies were immobilized, leading to the formation of immuno-sandwich conjugates according to the specific antigen–antibody binding on the test line, whereas excess composite-antibody further migrated toward the absorption pad. The selectivity of the functional nanoparticle depends on the antibody coupled with nanoparticles. In our study, the high specificity of anti-PCT monoclonal antibody could offer the high selectivity to the functional nanoparticle. The fluorescence signal of composite nanoparticles on the test line was observed by the fluorescence detector, which has a lightening of 365 nm LED lamp, at 15 min after the addition of analytes. Quantitative detection was realized by recording the PL intensity of nanoparticles captured on the test line. Before use, the PCT standard was diluted into a series of the concentration of the solution. The fluorescence signals were recorded by test strip reader and digital camera. The resulting calibration plots were linear as shown in Fig. 6(a); the correlation coefficients was 0.9788. The corresponding calibration plot of response *versus* PCT concentration was linear over the 0–10 ng mL^{-1} range and was suitable for quantitative analysis. Meanwhile, fluorescence images were also easily observed as shown in Fig. 6(b). We observed no signal in blank test, while proportional changed in fluorescence brightness of the test lines associated with the concentration of PCT. Such an observation was expected because the test line captures more composite-antibody when the analyte concentration was higher. The increased fluorescent signal strength at different PCT concentrations allowed us to study on rapid and quantitative analysis for PCT for clinical diagnosis. Furthermore, a red signal band from the target concentration as low as 0.1 ng mL^{-1} could be easily seen even with visual inspection. Over all, the achieved composite nanoparticles in this study were demonstrated to be a sensitive and reliable label material for such a bioassay.

4. Conclusions

In conclusion, using the LbL self-assembly technique and a multi-layer protection method, biocompatible SiO_2@PDDA@QDs@SiO_2@OTMS@PMAH composite nanoparticles were successfully prepared, and the material exhibited a high fluorescence intensity and good colloidal stability. We also confirmed the suitability of achieved nanoparticles for *in vitro* use by monitoring the highly amplified fluorescence signals from nanoparticles-labelled PCT. Further development and optimization of this technology should offer new opportunities to fundamental biophysics as well as clinical diagnostics.

Acknowledgements

The authors gratefully acknowledge the support of the National Natural Science Foundation of China (no. 21201055 and no. 61474037), Program for Science & Technology Innovation Talents in Universities of Henan Province (no. 14HASTIT009), Basic and cutting-edge technology research projects of Henan Province (no. 142300413207), and Program for Changjiang Scholars and Innovative Research Team in University (no. PCS IRT1126).

 This journal is © The Royal Society of Chemistry 2015

Published on 12 December 2014. Downloaded by Michigan State University on 21/01/2016 06:19:26.

Notes and references

1 R. Walt, *Science*, 2000, **287**, 451–452.
2 W. Ma, H. T. Liu, X. P. He, Y. Zang, J. Li, G. R. Chen, H. Tian and Y. T. Long, *Anal. Chem.*, 2014, **86**, 5502–5507.
3 H. L. Zhang, X. L. Wei, Y. Zang, J. Y. Cao, S. Liu, X. P. He, Q. Chen, Y. T. Long, J. Li, G. R. Chen and K. Chen, *Adv. Mater.*, 2013, **25**, 4097–4101.
4 Y. Zhang, J. Qian, D. Wang, Y. Wang and S. He, *Angew. Chem., Int. Ed.*, 2013, **52**, 1148–1151.
5 U. Resch-Genger, M. Grabolle, S. Cavaliere-Jaricot, R. Nitschke and T. Nann, *Nat. Methods*, 2008, **5**, 763–775.
6 L. Wang, W. Chen, W. Ma, L. Liu, W. Ma, Y. Zhao, Y. Zhu, L. Xu, H. Kuang and C. Xu, *Chem. Commun.*, 2011, **47**, 1574–1576.
7 X. L. Sun, B. Zhu, D. K. Ji, Q. B. Chen, X. P. He, G. R. Chen and T. D. James, *ACS Appl. Mater. Interfaces*, 2014, **6**, 10078–10082.
8 X. P. He, Q. Deng, L. Cai, C. Z. Wang, Y. Zang, J. Li, G. R. Chen and H. Tian, *ACS Appl. Mater. Interfaces*, 2014, **6**, 5379–5382.
9 Y. Zhu, Z. Li, M. Chen, H. M. Cooper and Z. P. Xu, *Chem. Mater.*, 2012, **24**, 421–423.
10 B.-H. Jun, D. W. Hwang, H. S. Jung, J. Jang, H. Kim, H. Kang, T. Kang, S. Kyeong, H. Lee, D. H. Jeong, K. W. Kang, H. Youn, D. S. Lee and Y.-S. Lee, *Adv. Funct. Mater.*, 2012, **22**, 1843–1849.
11 X. P. He, R. H. Li, S. Maisonneuve, Y. Ruan, G. R. Chen and J. Xie, *Chem. Commun.*, 2014, **50**, 14141–14144.
12 Q. Ma, I. C. Serrano and E. Palomares, *Chem. Commun.*, 2011, **47**, 7071–7073.
13 Y. He, Y. Su, X. Yang, Z. Kang, T. Xu, R. Zhang and S. T. Lee, *J. Am. Chem. Soc.*, 2009, **131**, 4434–4438.
14 B. H. Jun, G. Kim, M. S. Noh, H. Kang, Y. K. Kim, M. H. Cho, D. H. Jeong and Y. S. Lee, *Nanomedicine*, 2011, **6**, 1463–1480.
15 T. Song, Q. Zhang, C. Lu, X. Gong, Q. Yang, Y. Li, J. Liu and J. Chang, *J. Mater. Chem.*, 2011, **21**, 2169–2177.
16 A. T. Nagaraja, A. Sooresh, K. E. Meissner and M. J. McShane, *ACS Nano*, 2013, **7**, 6194–6202.
17 S. Beyer, W. C. Mak and D. Trau, *Langmuir*, 2007, **23**, 8827–8832.
18 Y. Chen, B. Jiang, Y. Xiang, Y. Chai and R. Yuan, *Chem. Commun.*, 2011, **47**, 7758–7760.
19 G. Decher, *Science*, 1997, **277**, 1232–1237.
20 F. C. Cebeci, Z. Wu, L. Zhai, R. E. Cohen and M. F. Rubner, *Langmuir*, 2006, **22**, 2856–2862.
21 M. Kuang, D. Wang, H. Bao, M. Y. Gao and M. Jiang, *Adv. Mater.*, 2005, **17**, 267–270.
22 Y. Gong, M. Y. Gao, D. Wang and H. Mohwald, *Chem. Mater.*, 2005, **17**, 2648–2653.
23 F. Erogbogbo, K.-T. Yong, I. Roy, G. Xu, P. N. Prasad and M. T. Swihart, *ACS Nano*, 2008, **2**, 873–878.
24 J.-H. Park, L. Gu, G. Maltzahn, E. Ruoslahti, S. N. Bhatia and M. J. Sailo, *Nat. Mater.*, 2009, **8**, 331–336.
25 R. Gui and X. An, *RSC Adv.*, 2013, **3**, 20959–20969.
26 B. Zhang, R. Hu, Y. Wang, C. Yang, X. Liu and K.-T. Yong, *RSC Adv.*, 2014, **4**, 13805–13816.
27 H. Shen, H. Wang, Z. Tang, J. Z. Niu, S. Lou, Z. Du and L. S. Li, *CrystEngComm*, 2009, **11**, 1733–1738.
28 J. Riegler and T. Nann, *Anal. Bioanal. Chem.*, 2004, **379**, 913–919.
29 C. Zhou, H. Yuan, X. Wang, H. Shen, Y. Guo, L. Xu, F. Wu, L. Ma and L. S. Li, *Sci. Adv. Mater.*, 2013, **5**, 285–294.
30 G. H. Bogush, M. A. Tracy and C. F. Zukoski IV, *J. Non-Cryst. Solids*, 1988, **104**, 95–106.
31 R. Ashayer, M. Green and S. H. Mannan, *J. Nanopart. Res.*, 2010, **12**, 1489–1494.
32 N. Insin, J. B. Tracy, H. Lee, J. P. Zimmer, R. M. Westervelt and M. G. Bawendi, *ACS Nano*, 2008, **2**, 197–202.
33 A. H. Lu, G. P. Hao and Q. Sun, *Angew. Chem., Int. Ed.*, 2011, **50**, 9023–9025.
34 P. H. Zhang, J. T. Cao, Q. H. Min and J. J. Zhu, *ACS Appl. Mater. Interfaces*, 2013, **5**, 7417–7424.
35 Z. Popović, W. Liu, V. P. Chauhan, J. Lee, C. Wong, A. B. Greytak, N. Insin, D. G. Nocera, D. Fukumura, R. K. Jain and M. G. Bawendi, *Angew. Chem.*, 2010, **122**, 8831–8834.
36 S. Liaudat, E. Dayer, G. Praz, J. Bille and N. Troillet, *Eur. J. Clin. Microbiol.*, 2001, **20**, 524–527.
37 M. Oppert, A. Reinicke, C. Müller, D. Barckow, U. Frei and K.-U. Eckardt, *Resuscitation*, 2002, **53**, 167–170.
38 Z. Jin and N. Hildebrandt, *Trends Biotechnol.*, 2012, **30**, 394–403.